https://doi.org/10.5194/egusphere-2025-5884
Preprint. Discussion started: 19 January 2026

An internally consistent framework for calculating cascading probabilistic earthquake risk and its application to a case study in New Zealand

Jose Moratalla, David Burbidge, Jean Roger, Katie Jones, Angela Griffin, Christof Mueller, Uma Ashok, Finn Scheele, Yaseen Mahmood, Edith Bretherton

Earth Sciences New Zealand, Lower Hutt, New Zealand

Correspondence to: moratalla.jmm@gmail.com

Abstract.

Quantifying the combined effects of earthquakes and their cascading hazards is essential for realistic risk assessment, yet such approaches remain limited in practice. Dynamic frameworks that explicitly correlate hazard intensities and their uncertainties across cascading perils provide more consistent and physically plausible impact estimates, offering greater value for resilience planning and risk management.

This study introduces a probabilistic risk assessment framework that integrates ground shaking, tsunami inundation, liquefaction, landslides, and their combined impacts into a unified modelling approach. The framework employs a fully correlated Monte Carlo–based hazard and damage model, ensuring that secondary perils and their effects on assets are conditionally linked to the triggering ground motions. This dynamic correlation maximises the representation of realistic damage scenarios.

The framework was tested in Napier, a city of 65,000 inhabitants situated directly above the Hikurangi Subduction Zone (HSZ), New Zealand's largest earthquake source with an estimated maximum credible magnitude of about Mw9.1. A 100,000-year stochastic catalogue of ruptures was generated and applied to ~30,000 residential buildings, with ground shaking, tsunami inundation, liquefaction severity, and landslide runouts explicitly modelled.

Results include damage state and damage ratio metrics for individual and combined perils. Earthquake shaking and liquefaction emerge as the dominant drivers of risk, followed by tsunami, lateral spreading, and landslides. These findings demonstrate the importance of capturing interdependent hazards in earthquake risk analysis. The framework provides decision makers, urban planners, and the (re)insurance sector with actionable metrics to guide resilience investments, refine underwriting, and minimise losses from cascading hazard events.

1.Introduction

Megathrust faults along the interface of subducting plates are responsible for the largest and most powerful earthquakes in the world, such as the 2004 Mw 9.3 Sumatra, 2010 Mw 8.8 Chile, 2011 Mw 9.1 Tohoku (Japan) and 2025 Mw 8.8 Kamchatka earthquakes. The Hikurangi Subduction Zone (HSZ), where the western Pacific Plate subducts under the Australian Plate off the east coast of the North Island of New Zealand, is thus potentially the most significant source of earthquake hazard and risk in New Zealand (Figure 1). An earthquake on the Hikurangi margin could trigger a cascading sequence of hazards that would have a significant impact on New Zealand communities, assets, and the national economy. For example, a large earthquake could trigger widespread

https://doi.org/10.5194/egusphere-2025-5884
Preprint. Discussion started: 19 January 2026

shaking, landslides, tsunami, fires, onshore ground subsidence, liquefaction, and further large earthquakes via a prolonged sequence of aftershocks. These effects could then create their own cascading series of further potential impacts. An earthquake on the HSZ is one of the most likely sources of offshore tsunami hazard for the several major New Zealand cities on the North Island (Power et al, 2022) and it is also one the largest single sources of seismic hazard to these cities, including New Zealand's capital city Wellington (Gerstenberger et al, 2022). To better prepare for, and mitigate, the effects of a large earthquake on the HSZ as many as possible of the combined perils that could be caused by the earthquake should therefore be considered.

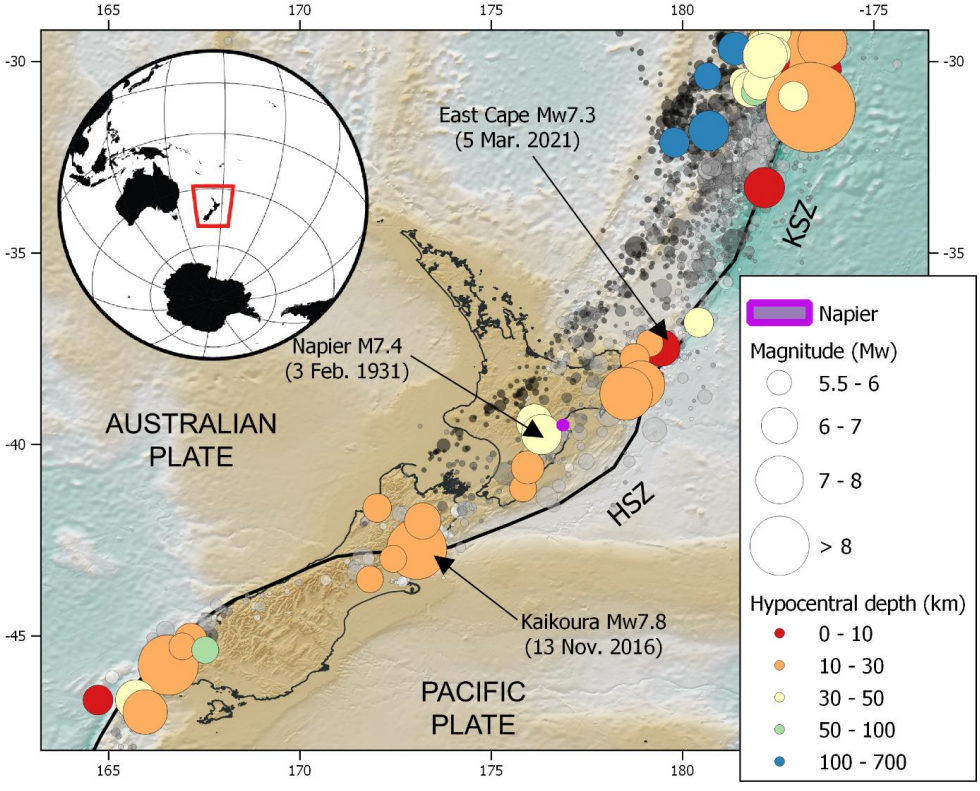

Figure 1: New Zealand within the seismotectonic context of subduction between the Pacific and the Australian tectonic plates; Grey circles symbolize the 5.0 ≤Mw ≤ 7.0 earthquakes since 1970; colored circles symbolize the Mw7.0+ earthquakes since 1900 (USGS catalogue)

Natural hazard risk assessments are traditionally carried out on individual hazards in isolation. This type of approach can be referred to as "single hazard" as opposed to a more holistic "multi-hazard" approach. Global scientific interest has been building over the last few years toward improving the quantification of risk by taking into account the potentially disastrous combination of multiple hazards, where the interactions between perils, or between cascading perils, are considered (e.g., Kappes et al 2012, Zariirova et al, 2019). For example, the necessity for a "holistic and multi-hazard approach to disaster risk management" (ISDR 2007) has been called for as part of the Hyogo Framework for Action. The 2011 Mw9.1 Tohoku earthquake and subsequent tsunami precipitating the Fukushima nuclear disaster (Pescaroli & Alexander 2015), the 2018 Mw7.5 Palu earthquake (severe shaking and tsunamis with extensive landslides, liquefaction and mudflows; Goda et al. 2019) and the 2008 Mw7.9

https://doi.org/10.5194/egusphere-2025-5884
Preprint. Discussion started: 19 January 2026

Wenchuan earthquake with seven episodes of extraordinary hazards impacting the Sichuan area (earthquake, multiple large landslides, dam-breaching floods, large-scale debris flows, severe sedimentation, change of river course, and flooding/scouring; Zhang et al. 2014; Fan et al. 2019) are three global examples highlighting the amplifying effect of cascading and multisource hazard systems. New Zealand has also experienced the disruptive effect of multi-hazards and cascading effects. For example, in the 2010–2012 Canterbury earthquake Sequence (ground shaking, landslides and liquefaction) and during the 2016 Kaikoura earthquake (earthquake shaking, landslides, tsunami, landslide dams and floodplain subsidence; Hughes et al. 2015; Robinson & Rosser 2017). Cyclone Gabriel 2023 caused flood and rainfall induced landslides in New Zealand´s North Island (ref) - plus cascading impact to infrastructure. Interactions within and across possible event chains can be complex and can involve a range of both geological and meteorological perils.

For the purposes of this paper, we define "cascading hazard" to be a hazard which has a causal link to the triggering event, possible via other perils. We are not including in this study the potential impact from coincidental perils, such as a tsunami that coincidentally arrives at the same time as equinox high tide or storm surge, or any changes to the risk due to long-term changes like, for example, the climate.

1.1 Multi-hazard Risk Assessments

Existing methods for multi-hazard risk assessment can be classified into qualitative, semi-quantitative and quantitative (Kappes et al. 2012, Zharikova et al. 2019). For qualitative methods the hazard intensity and recurrence interval limits are predefined and are then used to classify each of the perils into several classes. The value boundaries are usually determined by the location or objectives of the assessment. However, it is difficult to compare information from different sources in these types of assessments since most assessments have different criteria (Marzocchi et al. 2009).

Semi-quantitative methods typically use index-based approaches to represent risk on a standardized numerical scale (Kappes et al., 2012). With indices, the risk is given a score usually on a continuum. For example, this score could be calculated by multiplying the frequency of the peril per annum by the number of people (or the area) affected by it. If the index is needed for multiple perils combined, they are usually summed together from the individual perils. Both qualitative and semi-quantitative methods treat multiple perils as being independent. It is therefore difficult to consider the relationship between the perils within these frameworks.

In the context of risk reduction, quantitative methods offer advantage with the ability to quantify impact or risks and evaluate risk reduction measures thereby supporting decision making. Tilloy et al. (2019) did an extensive review of quantitative methods dealing with interconnected hazard and classified quantitative approaches into three techniques: stochastic, empirical, and mechanistic. Stochastic methods consider the statistical dependency between occurrence and intensity of hazards. For stochastic methods, the purpose is either to model the distribution of each individual hazard (Hao & Singh 2016; Liu et al. 2018), or to model the joint probability between hazards (Sadegh et al. 2018). The empirical method uses existing datasets to fit probability distributions. The accuracy of the fit can be quantified using dependence measures like Pearson or Spearman (Cdado, 2019), or regressions (Petroliagkis et al. 2016). The limitation of the empirical method is its dependency on data, and data is often limited in number due to rarity of mega events occurrence and damage information recorded. Mechanistic methods have been widely used by risk scientists for computing the potential impact of natural hazard events. However, the intensive nature of the computation makes them difficult to use for probabilistic risk assessment

https://doi.org/10.5194/egusphere-2025-5884
Preprint. Discussion started: 19 January 2026

and hence there can be bias toward a particular set of outcomes (Geist et al. 2009). Tocchi et al (2023) propose a multi-risk framework by integrating probabilistic hazard data (earthquakes and floods) with exposure and physical/social vulnerability indicators at the municipal level. A weighted, normalized aggregation produces a composite risk index to support disaster risk reduction prioritization.

1.2 Earthquake Hazard and Risk Assessment

Probabilistic earthquake risk assessments generally focus on one earthquake peril, typically seismic stochastic models with many of the parameters constrained through empirical methods and, sometimes, physical modelling. For probabilistic seismic hazard assessments, it is common practice to model the expected level of ground shaking and its variability due to site effects and aleatory uncertainty using ground motion prediction equations (GMPEs) across a region. Examples of these types of models span local (e.g., Burbidge et al, 2019a), national (e.g., Burbidge et al, 2012, Leonard et al, 2014, Gerstenberger et al, 2022) to global scale (e.g., Johnson et al, 2023).

It is much rarer for a probabilistic earthquake impact or risk assessment to consider a combination of earthquake induced perils. The most common method to incorporate the cascading effects of earthquakes is to focus on one or two earthquake scenarios and cascades (e.g., Power et al., 2018; Burbidge et al., 2019a; Kianrad et al., 2019). These are often done for a particular cascade of secondary effects (e.g., Power et al, 2018) in a deterministic or expert judgment-based approach or are done probabilistically but without fully quantifying the uncertainty and variability in the final loss estimates (e.g., Kianrad et al, 2019). The paper by Iannacone et al. (2024) introduces a simulation-based methodology to generate multi-hazard event sets over a system's life cycle, accounting for Level 1 (occurrence-based) interactions. Utilizing competing Poisson processes and sequential Monte Carlo sampling, the approach models concurrent, triggering, and altering interactions among hazards, producing realistic event sequences.

Two earthquake-induced perils that have been combined to calculate the combined probabilistic losses are those from strong ground shaking and tsunami (e.g., Goda 2020). In Goda (2020) the earthquake occurrence was represented by a set of multiple renewal models, implemented using a logic-tree approach, whereas earthquake rupture characterization is based on stochastic source models with variable fault geometry and heterogeneous slip distribution. By integrating these hazard components with seismic and tsunami fragility functions, the author calculated the time dependent multi-hazard loss potential from the combined impact of ground shaking and tsunami for some coastal communities in Japan. However, that study only considers the direct losses caused by shaking, not the losses caused by the cascading impacts of shaking such as liquefaction and earthquake induced landslides, both of which have been commonly observed in New Zealand following large earthquakes (e.g., during the 2010-2011 Canterbury Earthquake Sequence and the 2016 Kaikoura earthquake).

One probabilistic approach that captures the uncertainties in the ground motion modelling and its variability across the sites, the triggered cascading hazards, and the uncertainties in the asset's performance for a specific earthquake is presented by Moratalla and Uma (2023). In that study they first created an event tree of possible cascades from a Mw8.4 earthquake offshore Napier and then used Monte Carlo Simulation to determine a range of possible series of disruption outcomes to the road network for that specific earthquake. The study included the combined effect of shaking, liquefaction, lateral spreading, landslides and building collapse on the road network, but did not include tsunamis or consider a range of possible earthquakes. It thus could not calculate impact metrics such as

https://doi.org/10.5194/egusphere-2025-5884
Preprint. Discussion started: 19 January 2026

annualized probabilistic loss or risk exceedance curves from the combined effects of these earthquakes induced perils which require assessment of the risk across a range of earthquakes, rather than just one scenario.

Dunant et al. (2021) proposed a novel method for probabilistic cascading multi-hazard risk assessments using graph theory. The framework was tested in Franz Josef, New Zealand, and included impacts from earthquakes, landslides, and floods to housing and road infrastructure. One major advance provided by that study was the inclusion of non-dependent perils such as geological and meteorological hazards in a multi-hazard approach capable of combining them.

1.3 Objectives of this study

The work presented herein aims to first create a probabilistic framework for quantitatively estimating the combined impact, in terms of physical damage states and corresponding damage ratios (DRs), from earthquakes resulting from one or more faults' ruptures. The impacts will include those caused by the ground shaking, the tsunamis produced by the earthquakes and the cascading effects caused by the ground shaking (i.e. landslides, liquefaction and lateral spreading). The uncertainty in the hazards, and the damage they cause, will be concatenated (i.e., combined) using a Monte Carlo Simulation approach, described in detail in Sect. 2.

The key advantage, and novel, of this proposed framework is that it generates hazard intensities that are internally consistent across all perils within each earthquake event. This would allow the creation of realistic, event-driven cascading hazard scenarios where secondary impacts were conditionally linked to the primary seismic event parameters. The process would be repeated across all stochastic event sets (SES), enabling the construction of long-term, statistically robust hazard and damage distributions that capture both frequency and interdependence among hazards.

We then demonstrate the framework through a case study for earthquakes occurring on the HSZ affecting the residential buildings in Napier City, New Zealand (see Sect. 3).

Potential users of these risk metrics include asset owners, emergency managers, and government agencies. These risk outputs could be utilized for various purposes, such as land and emergency planning, prioritizing mitigation efforts, enhancing preparedness and resilience against cascading earthquake hazards, as well as planning and budgeting for recovery.

2. Methodology

2.1 A Monte-Carlo based approach for cascading hazards

In this study, we propose a Monte Carlo Simulation (MCS)-based framework to estimate the impact of earthquakes and their cascading hazards on the built environment. The framework is designed to model the effects of ground shaking, liquefaction, tsunami inundation, lateral spreading, and earthquake-induced landslides, using a synthetic catalogue of earthquakes. The results generated include Damage States (DS), which represent discrete levels of structural damage ranging from slight to complete. These are harmonized across all perils using a unified five-level classification developed in this study, based on existing fragility models such as those in HAZUS (2013) and Suprasri et al. (2013). In addition, the framework estimates mean damage ratios (MDRs)—representing the proportion of repair cost relative to full replacement—assigned to each harmonized DS using values derived from the HAZUS methodology.

https://doi.org/10.5194/egusphere-2025-5884
Preprint. Discussion started: 19 January 2026

2.2 Required Inputs

The implementation of the framework requires the 6 following components:

(1) Earthquake Catalogue: A stochastic catalogue of earthquakes affecting the study area, including rupture geometries, magnitudes, and recurrence information. For example, in the case study presented in this study we use a 100,000-year synthetic catalogue of Hikurangi Subduction Zone (HKSZ) earthquakes, developed using Event-Based Probabilistic Seismic Hazard Assessment (PSHA), the magnitude-frequency distribution (MFD) based on the 2022 New Zealand National Seismic Hazard Model (Gerstenberger et al., 2022) and implemented in OpenQuake (GEM, 2019).

(2) Ground Shaking Footprints: Ground motion intensity fields (e.g., Peak Ground Acceleration, PGA) generated for each event in the earthquake catalogue using Ground Motion Prediction Equations (GMPEs).

(3) Tsunami Inundation Depths: Inundation models triggered by each earthquake rupture capable of inundating the region of interest, providing water depth footprints.

(4) Cascading Ground Shaking Hazard Models: These include models for earthquake-induced landslides, lateral spreading, and liquefaction, which compute hazard intensities conditionally based on ground shaking.

(5) Fragility Functions: Harmonised peril-specific fragility models that relate hazard intensities to structural damage probabilities for different building types.

(6) Exposure Model: A dataset of buildings including location and construction characteristics, used to assign appropriate fragility functions.

2.3 Framework Workflow

Each earthquake in the catalogue is analysed using an MCS-based approach, which simulates damage from each individual peril and the combined effects of cascading hazards. The overall procedure, detailed in steps 1–9 and illustrated in Figure 2, is as follows:

1) **Event Selection:** A single earthquake event is selected from the stochastic catalogue (see Sect. 3.1).
2) **Shaking Intensity Modeling:** GMPEs are used to generate a ground shaking footprint (e.g., PGA, PGV) for the event at all exposure locations.
3) **Tsunami Inundation Modeling:** The earthquake ruptures are used to model tsunami generation and inundation depths, which are mapped to exposed assets (Sect. 3.3).
4) **Liquefaction Severity Modeling:** Liquefaction Severity Number (LSN) is calculated using local geotechnical conditions and shaking intensity (Tonkin & Taylor, 2013). LSN is sampled from a Poisson distribution within predefined susceptibility zones (Sect. 3.2.3).
5) **Lateral Spreading Modeling:** Lateral Displacement Index (LDI) is calculated per site using geotechnical data, slope angle, distance to a free face, and shaking intensity (Zhang et al., 2004). The resulting displacements are assigned to exposed buildings (Sect. 3.2.4).
6) **Landslide Modeling:** Landslide probabilities (EILP) are calculated from an earthquake-induced landslide susceptibility model to identify potential landslide source areas (Massey et al. 2021b, 2022). Landslide runout modeling identifies potential debris-inundation areas should a landslide occur (Brideau et al. 2020, 2021; Massey et al. 2021a). The resulting probabilities are assigned to exposed buildings (Sect. 3.2.5).
7) **Damage Estimation:** For each peril, the corresponding hazard intensity at each building is passed to the assigned fragility function to compute damage state (DS) probabilities. A uniform random number is used to sample the final DS from these probabilities.

https://doi.org/10.5194/egusphere-2025-5884
Preprint. Discussion started: 19 January 2026

8) **Damage State Harmonization:** Damage states from all perils are combined into a single harmonized damage state for each asset, reflecting the aggregated effects of shaking, tsunami, and secondary seismic hazards (Sect. 3.2.7).

9) **Damage Ratio Assignment to Damage States:** Once the harmonized damage state (DS) is determined for each asset, a corresponding damage ratio is assigned to represent the proportion of structural loss. This is done by mapping each DS to a predefined mean damage ratio (MDR), following established relationships such as those proposed in the HAZUS methodology (FEMA, 2020). The MDR values vary by building type and occupancy class, and are typically expressed as a fraction of total replacement cost (e.g., DS1 = 2%, DS5 = 100%). In this framework, damage ratios are sampled from a defined distribution (e.g., triangular or normal) centered on the mean, enabling further use in loss estimation or economic impact analysis if desired.

For every event in the catalogue, multiple Monte Carlo Simulations (MCS) are performed to sample the hazard intensities from their uncertainty distributions and damage states are also sampled from their corresponding damage state probabilities, resulting in randomly sampled damage state scenarios from every simulation. The probabilistic sampling in the MCS allows the generation of a number of different damage scenarios. The number of MCS´s required to achieve stable mean damage estimates for each event in the catalogue can be determined via convergence analysis. Due to the inclusion of multiple hazards and uncertainty sources, the minimum number of scenarios (N) needed for convergence is typically higher than in single-peril models.

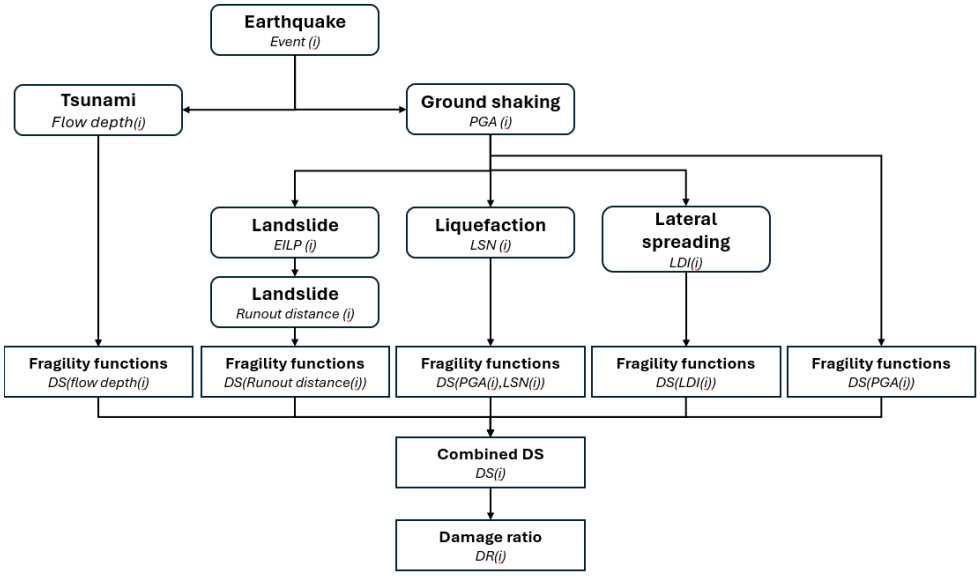

Figure 2: Damage state (DS) and Damage ratio (DR) calculation diagram for each simulation (i) performed for every event in the stochastic catalogue.

https://doi.org/10.5194/egusphere-2025-5884
Preprint. Discussion started: 19 January 2026

3. Case study: Napier City

3.1 Introduction

Napier City was selected as a pilot study area to test the cascading hazards framework developed in this work. Situated on the eastern coast of New Zealand's North Island, the city lies directly above the Hikurangi Subduction Zone interface (Williams et al., 2013) and less than 200 km from the subduction trench, making it highly exposed to seismic and tsunami hazards, as well as to cascading effects arising from intense ground shaking (as shown by the historical examples in S1)

Liquefaction represents a major threat due to the prevalence of loose sedimentary deposits and a high groundwater table, while the proximity of water channels to residential areas enhances the potential for lateral spreading. The city also exhibits potential for landslides triggered by seismic shaking, particularly on surrounding slopes. Furthermore, its coastal position facing the Hikurangi Subduction Zone increases vulnerability to earthquake-induced tsunamis, as well as to possible submarine landslide-generated tsunamis. The coexistence and interdependence of these hazards underscore Napier's pronounced susceptibility to cascading impacts, justifying its selection for the application and validation of the proposed framework. Sect. 3, along with the corresponding Supplementary Material (S1 to S8), include the details of the hazards, exposure and fragility modelling for this case study.

3.2 Hazard modelling

3.2.1 Earthquake

For this case study we generated a 100,000-years stochastic earthquake catalogue using the Hikurangi Subduction Zone (HSZ) as the sole seismic source (Williams et al., 2013). The catalogue was produced with OpenQuake (GEM, 2019), using the Hikurangi Magnitude–Frequency Distribution (Gutenberg–Richter a and b values) based on the Distributed Seismicity Model of the New Zealand National Seismic Hazard Model (Rollins et al., 2022). The HSZ was assumed capable of hosting events up to Mw 9.1, and Ground Motion Prediction Equations (GMPEs) for subduction interface events were selected following the latest model recommendations (Gerstenberger et al., 2022), with site effects incorporated through the mean shear-wave velocity in the upper 30 m (V_{S30}). The subduction interface geometry, recurrence implementation, and ground-motion modelling details are described in more detail in S2.

3.2.2 Tsunami

To calculate the tsunami inundation, we first stochastically generate slip distributions for a set of earthquakes of different magnitudes at a set of points distributed along the HSZ. Simulating tsunami inundations with a hydrodynamic model at the resolution used in this study comes at a considerable computational cost. This meant that we had to limit the number of tsunami models in order for the project to be tractable. To help with this, the scenarios were carefully selected to include only those ruptures most likely to generate inundation in Napier, taking into consideration the city's unique topographic setting, notably which coast acts as a natural barrier against tsunamis of small to moderate heights (e.g., elevated topography and presence of large coastal gravel ridges). In the end, 33 scenarios were selected spaced with centroids spread along the HSZ. The scenarios ranged in moment magnitude from 7.5 to 9.1. For each of these 33 scenarios, 10 variations of non-uniform slip distribution were

https://doi.org/10.5194/egusphere-2025-5884
Preprint. Discussion started: 19 January 2026

calculated, and the resulting 330 models were then run through to inundation using the tsunami hydrodynamic model, COMCOT on a set of nested grids, including a 10m resolution grid covering Napier and its neighbourhood. The flow depth at each building in the city was then extracted from each of these tsunami scenarios. During the MCS process, described below, the tsunami scenario for a particular earthquake realisation is randomly chosen from the 10 possible slip variations in the tsunami inundation model library which were closest to the epicentre and magnitude of the earthquake in the stochastic catalogue. For the purposes of this case study, each of the 10 possible slip variations is assumed to be equally likely. Further details of how the tsunami scenarios were created can be found in S3.

3.2.3 Liquefaction

Liquefaction susceptibility zones defined by Rosser and Dellow (2017) were adopted to represent the spatial variability of liquefaction potential across Napier City. These zones, derived from geomorphological and sedimentological mapping, were used to delineate six liquefaction susceptibility areas in this study (Figure 3a). To enhance the confidence in the 2017 maps, seventeen additional cone penetration tests were analysed for liquefaction susceptibility, using the existing parameters from the 2017 work and new knowledge gained since then (Griffin 2024).

For each susceptibility zone, borehole data were compiled and grouped, and their properties within the upper 10 m were analyzed to characterize material variability. The corresponding CPT-derived Liquefaction Severity Number (LSN, Tonkin & Taylor, 2013) values were fitted to normal distributions, enabling a probabilistic representation of LSN variability within each zone. This statistical approach captures the spatial variability in liquefaction response across Napier and is used in the subsequent hazard and risk analyses.

Further methodological details, including CPT processing, software implementation, and the derivation of LSN distributions under variable earthquake scenarios, are provided in S4.

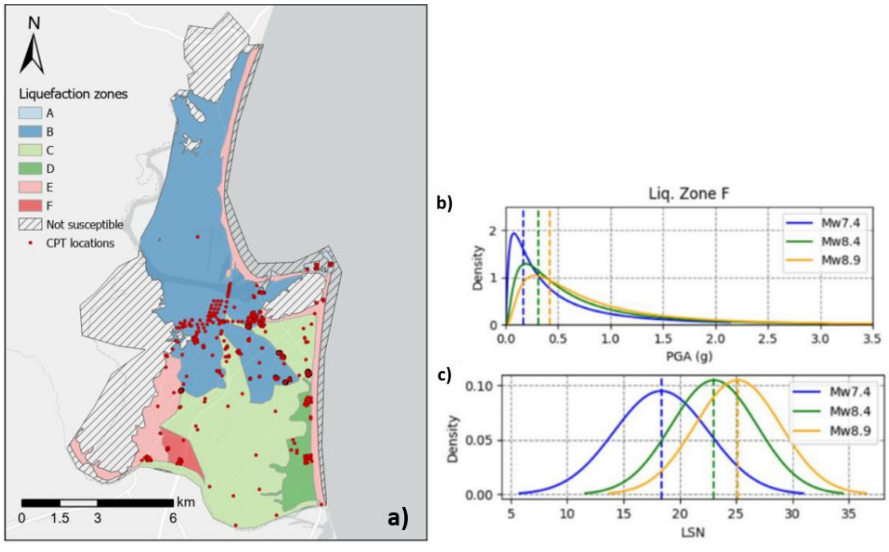

Figure 3: a) The Liquefaction Zones in the study are and the CPT locations that were used to derive them. b)PGA, c) LSN distributions for zone F, for three example earthquake scenarios. Results for the rest of zones are shown in the Figure S7.

https://doi.org/10.5194/egusphere-2025-5884
Preprint. Discussion started: 19 January 2026

3.1.4 Lateral spreading

Liquefaction induced lateral displacements (LD) were estimated based on the method proposed by Zhang et al (2004) to first calculate the Lateral Displacement Index (LDI) and further include the influence of ground slope with and without a free face. This approach is recommended to be used for earthquake magnitudes between 6.4 and 9.2, and peak ground accelerations between 0.19 and 0.6 g. Areas with potential for lateral spreading were identified by mapping free faces and surface slope in areas with liquefaction potential and mapping their attributes to the building locations. Then, the Lateral Displacement Index (LDI) was estimated using the approach by Zang et al, (2004). Further information about how this peril was calculated is also provided in S5.

3.1.5 Landslides

While most of the study area across Napier is flat, the areas in, or adjacent, to steep topography are potentially vulnerable to landslide impact. The terrestrial risk from Earthquake-induced Landslides (EIL) was estimated based on the methods proposed by Brideau et al. (2020, 2021) and Massey et al. (2021a). Underwater landslides, which could potentially cause a tsunami, are not considered in the present study.

Co-seismic landslide probabilities were modelled using the New Zealand Earthquake-Induced Landslide Forecast Tool (Version 2.0) (Massey et al., 2021b; 2022), which estimates regional landslide probability as a function of ground shaking intensity, topography and geology. The model was run for ten uniform PGA levels (0.2–3.0 g) to capture the range of shaking expected from the maximum event in the stochastic catalogue (Mw 9.1 HSZ scenario).

Slope units were delineated from the NZ 8 m DEM, which were refined into source regions using empirical relationships between slope, local slope relief, and landslide occurrence derived from the Kaikōura Earthquake Inventory (Jones et al., 2024). For each source region, the maximum landslide volume class was defined, and the probability of each class was determined from the Kaikōura EIL frequency-area distribution.

Landslide runout extents were modelled using empirical landslide runout relationships, which use the Fahrböschung angle to estimate the runout distance for each volume class (Brideau et al. 2020, 2021; Massey et al. 2021a). Only open-slope dry rock and debris avalanches (OSD) were considered, as they are the most representative earthquake-triggered landslide type. Buildings intersecting either the landslide source regions or debris-inundation polygons were identified for subsequent risk simulations (Figure 4). Further methodological details for each of these steps are presented in S6.

https://doi.org/10.5194/egusphere-2025-5884
Preprint. Discussion started: 19 January 2026

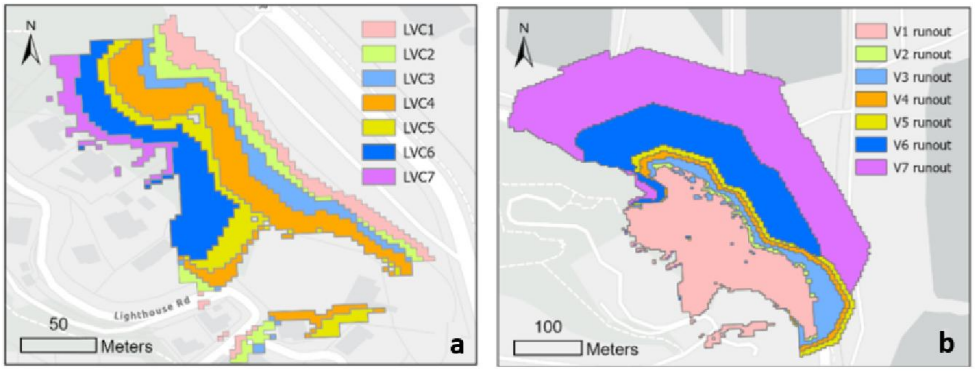

Figure 4: a) Example of the seven landslide volume classes within a single source region. b) Example of the runout for each of the seven landslide volume classes within a single source region. The slope units, source regions and landslide volume classes are defined

3.1.6 Exposure modelling

A national building inventory developed by Scheele et al. (2023) was used to represent the residential building stock in the study area. The dataset provides building locations and key structural attributes required for risk modelling. From this inventory, 38,344 residential buildings within the Napier City Territorial Authority were extracted for analysis.

Residential buildings are primarily exposed to earthquake ground shaking, with additional exposure to liquefaction, tsunami, lateral spreading, and landslide hazards. Due to the soil conditions across Napier City, liquefaction is expected to be the most significant secondary hazard (Table 2). Further details on the building inventory compilation and data matching procedures are provided in S7.

Table 1: Buildings exposure against the different hazards

	No. buildings	%
All	38344	100 %
Earthquake shaking	38344	100%
Liquefaction	33905	88%
Tsunami	17073	45%
Lateral spreading	15478	18%
Landslide	6612	17%

3.1.7 Fragility/vulnerability modelling

Building fragility functions express the probability of exceeding a given damage state (DS) for a specified intensity measure (e.g., PGA). Damage states qualitatively describe structural damage, typically ranging from minor to complete, with two or three intermediate levels commonly defined (e.g., HAZUS 2.1). Fragility models

https://doi.org/10.5194/egusphere-2025-5884
Preprint. Discussion started: 19 January 2026

are developed using either empirical data, based on observed post-event damage, or analytical methods, where structural response to hazard demand is modelled (Xin et al., 2020).

Earthquake damage was estimated using HAZUS 2.1 functions, which define four structural damage states (slight, moderate, extensive, complete) for major building types. Buildings in Napier were classified by material, height, and age. Each fragility curve follows a lognormal distribution, and damage ratios (DRs) were assigned as: slight = 0.15, moderate = 0.3, extensive = 0.7, complete = 1.0.

Tsunami damage used empirically derived fragility functions from Supprasri et al. (2013), based on post-2011 Great East Japan Tsunami data. Six damage states were simplified into four representative DRs: minor = 0.1, moderate = 0.2, major = 0.7, and complete/collapse = 1.0.

Liquefaction effects were modelled as an aggravation factor (Δ) applied to earthquake fragility exceedance probabilities, using LSN as a proxy for severity: LSN (0–15] Δ=1.1; (15–25] Δ=1.3; >25 Δ=1.5, capped at 100%.

Lateral spreading damage was modelled using permanent ground displacement (PGD)–based fragility functions from HAZUS, with four damage states consistent with the ground-shaking model.

Landslide impacts were represented using a rule-based approach, classifying damage by the degree of overlap between the building footprint and the runout area: no overlap = no damage; partial overlap = moderate; full overlap = complete.

In multi-hazard risk assessment, particularly when evaluating cascading impacts from cascading hazards, a key challenge arises from the need to integrate damage estimates derived from different fragility models, each with their own damage state definitions and granularity. This process, known as damage state harmonization, involves mapping and aligning the distinct damage classifications used for different perils into a unified framework.

The harmonized damage stated are summarised in table 3. Detailed description of the harmonized damage states are included in S7.

Table 2: Unified five-level damage state framework developed to integrate disparate fragility model outputs for shaking, liquefaction, lateral spreading, tsunami, and landslide hazards. The harmonization ensures consistency in structural damage interpretation across cascading hazard scenarios.

Harmonized DS	Label	Shaking	Liquefaction	Lateral Spreading	Tsunami	Landslide
DS1	Slight	Slight	Slight	Slight	Minor	No debris affects building
DS2	Moderate	Moderate	Moderate	Moderate	Moderate	No debris affects building
DS3	Severe	Extensive	Extensive	Extensive	Major	Debris affects part of the building footprint
DS4	Complete	Complete	Complete	Complete	Complete	Entire footprint covered by debris

https://doi.org/10.5194/egusphere-2025-5884
Preprint. Discussion started: 19 January 2026

DS5	Collapsed/ Washed away	— (implicit)	— (implicit)	— (implicit)	Collapsed / Washed away	— (implicit)

Damage Ratios (DRs) represent repair costs as a percentage of a building's replacement value. Because DRs vary with construction characteristics, damage severity, and repair practices, they are modelled as random variables rather than fixed values.

Damage Ratios (DRs) express repair costs as a percentage of a building's replacement value and were assigned to each asset based on the harmonized damage states from the cascading hazard framework. Mean DR values were adopted from the Structural Repair Cost Ratios in HAZUS (HAZUS, 2013), mapped to the five-level damage scale used in this study. Because HAZUS provides only mean values, uncertainty was represented using a triangular probability distribution with bounds of ±30% around the mean. During each Monte Carlo simulation, DRs were randomly sampled from this distribution to reflect variability in repair costs while maintaining consistency with standardized engineering assumptions.

This study focuses exclusively on structural damage; potential losses to non-structural elements and building contents are not included in the damage or cost estimates. It is also recognized that HAZUS damage ratios are primarily calibrated for earthquake-induced losses, whereas other hazards may produce different damage mechanisms and cost relationships. Future work should therefore incorporate peril-specific damage ratios to enhance the accuracy of multi-hazard impact assessments.

3.2 Convergence analysis

A convergence analysis was conducted to assess the statistical stability of mean damage ratios (MDR) derived from the stochastic seismic simulations. Convergence refers to the point at which the cumulative mean MDR stabilizes with minimal variation as the number of simulations increases—a principle rooted in Monte Carlo–based uncertainty quantification (Burt and Garman, 1971; Ata, 2007). Two convergence tests were performed.

The first evaluated site–event level convergence, where a single building was repeatedly exposed to a given earthquake event to determine the number of realizations required for MDR stability. The mean MDR stabilized within a ±2% threshold after approximately 120–180 simulations, so 200 simulations per event were modelled (Figure 5).

https://doi.org/10.5194/egusphere-2025-5884
Preprint. Discussion started: 19 January 2026

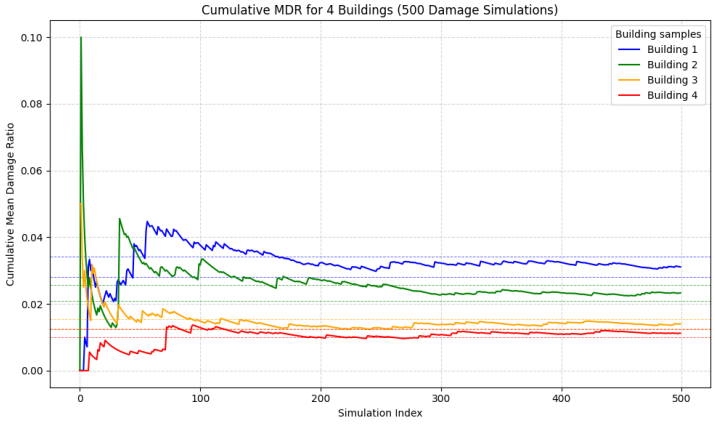

Figure 5: Cumulative mean damage ratio (MDR) for four representative buildings across 500 stochastic damage simulations of a single Mw7.15 earthquake event. Each curve shows the progressive average MDR per building, with horizontal dashed lines indicating ±2% bounds around the final cumulative MDR value.

The second test assessed catalogue-level convergence, examining how many unique events were required for the cumulative MDR to stabilize across the stochastic earthquake catalogue. The results show that stability was achieved within ±2% after 20,000–30,000 events, with full convergence reached at 45,000 events (Figure 6). These findings confirm that the 100,000-year event catalogue provides a statistically sufficient basis for robust risk estimation.

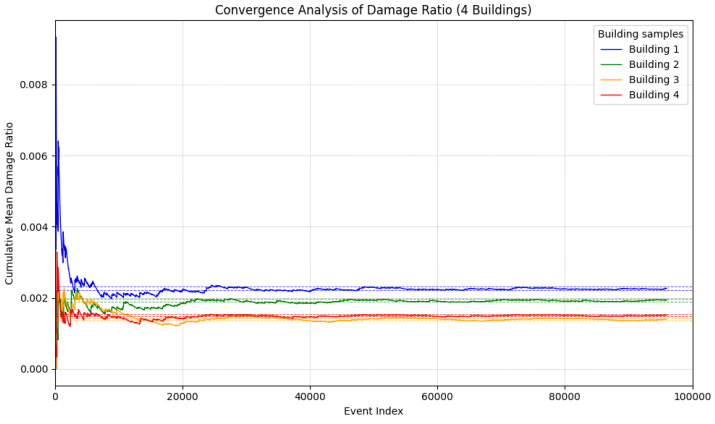

Figure 6: Cumulative Mean Damage Ratio (MDR) convergence for four representative buildings under the full stochastic earthquake catalogue. Each colored curve represents the evolving MDR as a function of the number of contributing events, while dashed lines indicate ±2% bounds from the final cumulative mean.

3.3 Results

The framework proposed in this work is capable of providing damage state (DS) level results and damage ratios (DR) at each asset location. Results can then be processed to present area-wide outputs such as regional damage state curves vs return period, mean damage ratios from combined and dissagregated perils, or annual average mean damage ratios.

https://doi.org/10.5194/egusphere-2025-5884
Preprint. Discussion started: 19 January 2026

Results for the case study proposed – impacts from the Hikurangi Subduction Zone earthquakes and cascading hazards to Napier City´s residential building portfolio- are presented as follows:

1. **Regional damage states:** Return period curves for damage states can be used to characterize urban resilience by quantifying the probabilities of structural damage over time. Results can be presented in the form of exceedance probability curves of different damage states and the proportion of buildings under a certain damage state at different return periods. The DS exceedance probability per year (P) is calculated as follows:

$$P\ (DS \geq x) = \frac{N_{buildings}(DS \geq x)}{N_{buildings}} \quad (3)$$

Then, the return periods are obtained as:

$$\boldsymbol{RP_i} = \frac{\boldsymbol{N_{years}+1}}{\boldsymbol{i}} \quad (4)$$

Where i is the i-th largest exceedance probability for damage state DS ≥ x.

Figure 7 illustrates the distribution of exclusive damage states (DS0–DS4) in Napier City as a function of return period for earthquakes on the HSZ. The bars indicate that the damage level increases with hazard intensity. Minor damage (DS ≥1) becomes noticeable beyond ~100-year events, while extensive damage and collapse (DS ≥3, DS ≥4) remain unlikely until return periods exceed ~500 years. At extreme return periods (10,000–100,000 years), the probabilities of higher damage states rise sharply, with DS ≥3 and DS ≥4 approaching or exceeding 50%, showing that severe shaking is required to trigger widespread collapses. The spacing between the curves emphasizes the greater fragility to slight damage compared to complete failure.

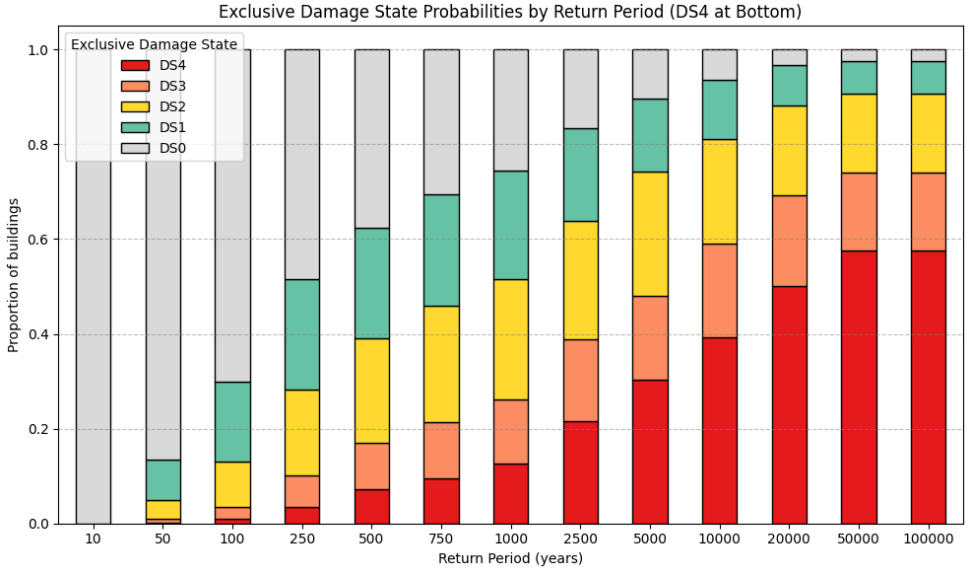

Figure 7: Proportion of buildings in the area of study at different damage states for different return periods.

2. **MDR Return Period curves**: Resulting mean damage ratios (MDR) can be presented as exceedance probability curves (EP curves) for a given time interval (e.g., 1 year), or return period curves, which represent the estimated period at which a given loss will be exceeded. Results can be disaggregated by

https://doi.org/10.5194/egusphere-2025-5884
Preprint. Discussion started: 19 January 2026

hazard and also combined in a MDR curve.

The MDR for an event j is calculated as:

$$MDR_j = \frac{1}{N_{buildings}} \sum_{i=1}^{N_{buildins}} DR_{ij} \quad (5)$$

Where DRij is the damage ratio for building i under the event j. Results per year can then be sorted by increasing MDR and RPs calculated as in Equation (4).

When disaggregating the results for each peril, results can be expressed relative to the total exposure in the area considered (Total mean damage ratio, TMDR), or relative to the areas exposed to the different hazards (Relative Mean Damage Ratio, RMDR). Each result provides a different view of the risk, the first, TMDR, shows how each hazard contributes, separately, to the expected losses ; the second, RMDR, presents how each hazard contributes to loss of its respective exposed buildings.

Figure 8 shows the TMDR and RMDR results for the Napier City case study. At the smaller return periods the losses are primarily from the ground shaking (red curve) and liquefaction (orange curve) as expected. At longer periods the losses from the other perils start to contribute to the total loss, with the losses from tsunami (blue curves) becoming comparable to ground shaking and liquefaction at very long return periods above about 10,000 years. The losses from EILs (green curves) are a relatively small proportion of the total loss, as shown by the TMDR figure, but this is mainly due to the relatively small amount of exposed assets to EILs in this case study region (Table 2). As shown by the RMDR curve, EILs start to impact buildings in their exposed area quite significantly for return periods above about 50-100 years.

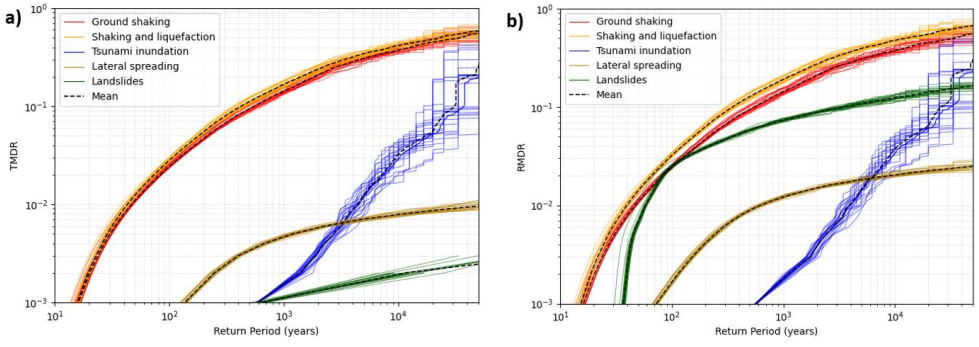

Figure 8: a) Total mean damage ratios (TMDR) and b) Relative mean damage ratios (RMDR) expected in Napier City disaggregated for earthquakes on the HSZ for each peril considered in this study.

3. **Annual average mean damage ratio (AAMDR):** We have also calculated the average annual MDR for the 100,000-years stochastic catalogue. The length of the catalogue was selected based on a convergence analysis, which concluded that 100,000 years was of a sufficient length. The AAMDR can be calculated as:

$$AAMDR = \sum_{j=1}^{N} P_j \cdot MDR_j \quad (6)$$

Where N is the total number of simulated hazard events, P_j is the annual probability of event j (typically $1/N$years if all events are equiprobable) and MDR is the mean damage ratio for an event j.

https://doi.org/10.5194/egusphere-2025-5884
Preprint. Discussion started: 19 January 2026

4. A 1 km regular grid was generated across the study area, and the average annual mean damage ratio (AAMDR) for all buildings within each subdivision was computed to map its regional distribution (Figure 9). Results show clear clustering of damage in areas with high building density (see Figure S9 for reference on exposure distribution) and where multiple hazards occur simultaneously. Additionally, zones identified as landslide-prone display elevated AAMDR values, indicating the significant influence of local topographic effects on the spatial pattern of cascading hazard impacts.

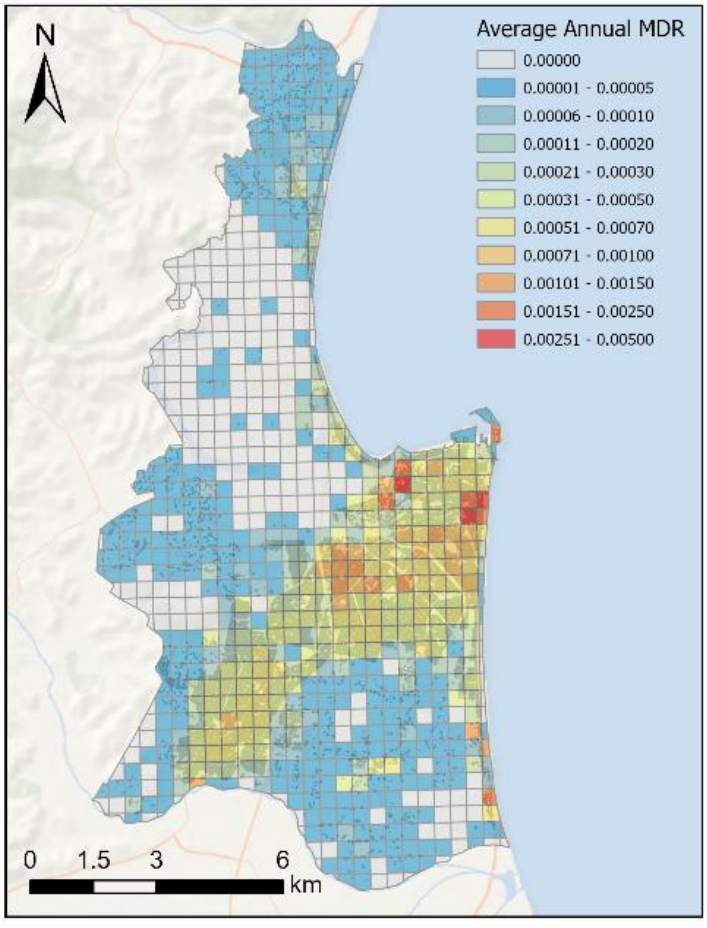

Figure 9: Regional distribution of the average annual mean damage ratio of combined effect of earthquakes on the HSZ and the cascading hazards considered in this study.

4.0 Discussion and conclusions

In this study we have described how to create an internally consistent framework for calculating earthquake risk, including both primary and secondary perils, and applied it to a case study region in Napier City, NZ. All hazard intensities and their associated damage states are sampled in a statistically coherent manner for each event within a Monte Carlo framework, preserving the physical and causal relationships among hazards. This makes a

https://doi.org/10.5194/egusphere-2025-5884
Preprint. Discussion started: 19 January 2026

difference with the more common alternative approach of simulating each hazard independently, adding the advantage of capturing the inter-hazard intensity correlations inherent to each event realization.

From the damage state analysis of the area of study (Figure 7), the building stock in Napier City appears able to withstand more frequent, moderate earthquakes with minor damage – most structures stay intact or only slightly affected in events up to ~100-year return period, which suggests a reasonable performance for everyday seismicity from the HSZ. However, the steep rise in damage probabilities and the shift toward predominantly severe damage at longer return periods indicate that the structures become increasingly fragile under tail events. In rare, large-magnitude earthquakes on the HSZ, well beyond the typical design level, damage is no longer distributed across lower states but concentrated in the most severe states (DS3–DS4), meaning widespread heavy damage and collapse caused by strong ground motion and the triggered cascading hazards. This concentration of expected damage in extreme events points to limited urban resilience against the very largest events – while the city might quickly recover from moderate quakes, a truly severe HSZ earthquake could overwhelm buildings and infrastructure. In summary, the results suggest that Napier City's buildings have a threshold of performance: they perform adequately under moderate hazard levels, but beyond that threshold the probability of extensive structural failure grows dramatically, posing a significant risk of catastrophic losses and challenging the city's ability to respond and recover.

Disaggregated MDR results confirm that earthquake shaking and liquefaction are the dominant damage drivers in Napier City for HSZ earthquakes, followed by tsunami, lateral spreading, and landslides (Figure 8). The city's proximity to the subduction interface makes it highly exposed to intense ground shaking, which emerges as the leading cause of losses.

Tsunami-related losses become comparable to shaking and liquefaction only at very long return periods, reflecting the low-frequency, high-consequence nature of large offshore ruptures. This behaviour is consistent with tsunami hazard curves (discussed and presented in S3) which show two main inflection points—around 0.3–0.5 m and 4–6 m flow depth. These correspond to, respectively, the early inundation of the Ahuriri estuary and the overtopping of a 4–6 m coastal gravel ridge. Only the largest simulated HSZ earthquakes exceed this ridge, explaining why severe tsunami damage is confined to the rarest events.

Liquefaction significantly amplifies shaking-induced damage because of Napier's highly susceptible geological conditions, confirmed by extensive geotechnical investigations. Its combined contribution with shaking dominates total losses across most return periods, consistent with historical evidence from the 1931 Mw 7.3 Napier earthquake.

Lateral spreading represents the second most relevant secondary hazard after liquefaction, particularly for intermediate return periods up to about 2,000 years. This effect is linked to the city's geomorphology—reclaimed land and stream corridors prone to liquefaction-induced lateral displacements that exacerbate structural damage during moderate to strong shaking.

Earthquake-induced landslides contribute the least to mean damage ratios due to the limited building exposure in susceptible zones. However, for assets located within these zones, landslides can still be the second most significant damage source, as illustrated in Figure 9.

This study shows that the proposed framework provides a robust, internally consistent means to quantify the impacts of earthquakes and their cascading hazards. The framework can support efforts to strengthen resilience, guide preparedness planning, and ultimately reduce the consequences of future earthquake events on communities.

https://doi.org/10.5194/egusphere-2025-5884
Preprint. Discussion started: 19 January 2026

5.0 Acknowledgments

This project was supported by the New Zealand Ministry of Business, Innovation and Employment (MBIE) through the Hazards and Risk Mitigation Programme's End-to-End Framework Flagship Project (Strategic Science Investment Fund, contract C05X1702). The authors would like to thank Biljana Lukovic for her assistance with the landslide hazard modelling, Saskia de Vilder for guidance about landslide hazard and risk analysis, Alex Dunant and Nicolas Pondard for their contribution at the early stages of this study.

The contact author has declared that none of the authors has any competing interests.

6.0 Author contributions

JM contributed to Conceptualization, Methodology, Software, Formal analysis, Investigation (seismic hazard, liquefaction, fragility, cascading hazards and risk modelling), Visualization, and Writing (original draft preparation). DB contributed to Conceptualization, Supervision, and Writing. JR contributed to Methodology, Investigation (tsunami modelling), and Writing. KJ contributed to Investigation (landslide modelling) and Writing. AG contributed to Investigation (borehole analysis) and Writing. CM contributed to Methodology and Investigation (tsunami modelling). SU contributed to Writing (review and editing). FS contributed to Investigation (exposure modelling). YM contributed to Software (code implementation support). EB contributed to Project administration and Visualization (framework dissemination).

7.0 References

Ata, M. Y.: A convergence criterion for the Monte Carlo estimates, Simul. Model. Pract. Theory, 15, 237–246, doi:10.1016/j.simpat.2006.12.002, 2007.

Brideau, M. A., Massey, C. I., Lukovic, B., and Morgenstern, R.: Deterministic mapping of potential landslide debris inundation in the Kaikōura District, GNS Sci. Consult. Rep., 2019/102, Lower Hutt, New Zealand, 2020.

Brideau, M. A., de Vilder, S., Massey, C., Mitchell, A., McDougall, S., and Aaron, J.: Empirical relationships to estimate the probability of runout exceedance for various landslide types, in: Understanding and Reducing Landslide Disaster Risk, Springer, Cham, doi:10.1007/978-3-030-60227-7_36, 2021.

Burbidge, D. R. (ed.): The 2012 Australian earthquake hazard map, Geosci. Aust. Rec., 2012/71, Canberra, 2012.

Burbidge, D. R., Moratalla, J. M., Goded, T., and Lukovic, B.: Probabilistic seismic hazard model for South Paray Wharf, Port Vila, Vanuatu, GNS Sci. Consult. Rep., 2019/153, 35 pp., 2019a.

Burt, J. M., and Garman, M. B.: Conditional Monte Carlo: A simulation technique for stochastic network analysis, Manag. Sci., 18, 207–217, doi:10.1287/mnsc.18.3.207, 1971.

Callaghan, F. R.: The Hawke's Bay earthquake: general description, N. Z. J. Sci. Technol., 15, 1–37, 1933.

Czado, C.: Dependence Measures, in: Analyzing Dependent Data with Vine Copulas, Springer, Cham, doi:10.1007/978-3-030-13785-4_2, 2019.

https://doi.org/10.5194/egusphere-2025-5884
Preprint. Discussion started: 19 January 2026

Dellow, G. D., Hengesh, J. V., Heron, D., Brown, L., and Hull, A. G.: Earthquake hazard analysis program: Stage II, Part II – Evaluation of liquefaction potential in the Hawke's Bay region, Inst. Geol. Nucl. Sci. Client Rep., 1999/6, Lower Hutt, New Zealand, 63 pp., 1999.

Dellow, G. D., Glassey, P. J., Lukovic, B., Wood, P. R., and Morrison, B.: Data sources of the New Zealand landslide database, EGS–AGU–EUG Joint Assembly, Nice, abstract #13867, 2003.

Dowrick, D. J.: Damage and intensities in the magnitude 7.8 1931 Hawke's Bay, New Zealand, earthquake, Bull. N. Z. Soc. Earthq. Eng., 8, 255–259, 1998.

Dunant, A., Bebbington, M., Davies, T., and Horton, P.: Multihazards scenario generator: a network-based simulation of natural disasters, Risk Anal., 41, doi:10.1111/risa.13723, 2021.

Fairless, G. J., and Berrill, J. B.: Liquefaction during historic earthquakes in New Zealand, Bull. N. Z. Natl. Soc. Earthq. Eng., 17, 280–291, 1984.

Fan, X., et al.: Earthquake-induced chains of geologic hazards: patterns, mechanisms, and impacts, Rev. Geophys., 57, 421–503, doi:10.1029/2018RG000626, 2019.

GEM: The OpenQuake-engine user manual, GEM Foundation, Pavia, Italy, 189 pp., doi:10.13117/GEM.OPENQUAKE.MAN.ENGINE.3.3.0, 2019.

Gerstenberger, M. C., Bora, S. S., Bradley, B. A., DiCaprio, C., Van Dissen, R. J., Atkinson, G. M., and Wotherspoon, L. M.: New Zealand National Seismic Hazard Model 2022 revision: model, hazard and process overview, GNS Sci. Rep., 2022/57, 106 pp., doi:10.21420/TB83-7X19, 2022.

Geist, E. L., Lynett, P. J., and Chaytor, J. D.: Hydrodynamic modeling of tsunamis from the Currituck landslide, Mar. Geol., 264, 41–52, doi:10.1016/j.margeo.2008.09.005, 2009.

Goda, K., Mori, N., Yasuda, T., Prasetyo, A., Muhammad, A., and Tsujio, D.: Cascading geological hazards and risks of the 2018 Sulawesi earthquake and sensitivity analysis of tsunami inundation simulations, Front. Earth Sci., 7, 261, doi:10.3389/feart.2019.00261, 2019.

Goda, K.: Multi-hazard portfolio loss estimation for time-dependent shaking and tsunami hazards, Front. Earth Sci., 8, 592444, doi:10.3389/feart.2020.592444, 2020.

Griffin, A. G.: Liquefaction analysis for selected locations in Napier–Hastings, GNS Sci. Rep., 2024/07, 2024.

HAZUS-MH 2.1 Committee, Earthquake et al.: HAZUS-MH 2.1 Earthquake Model Technical Manual, 2013.

Hao, Z., and Singh, V. P.: Review of dependence modeling in hydrology and water resources, Prog. Phys. Geogr., 40, 549–578, doi:10.1177/0309133316632460, 2016.

Hughes, M., Quigley, M., van Ballegooy, S., Deam, B., Bradley, B., Hart, D., and Measures, R.: The sinking city: earthquakes increase flood hazard in Christchurch, New Zealand, GSA Today, 25, 3–4, doi:10.1130/GSATG221A.1, 2015.

Johnson, K., et al.: Global Earthquake Model (GEM) Seismic Hazard Map (version 2023.1), doi:10.5281/zenodo.8409647, 2023.

Jones, K., et al.: Version 3.0 of the landslide inventory for the Mw 7.8 2016 Kaikōura earthquake, GNS Science, doi:10.21420/WX2X-H603, 2024.

Kappes, M. S., Keiler, M., von Elverfeldt, K., and Glade, T.: Challenges of analyzing multi-hazard risk: a review, Nat. Hazards, 64, 1925–1958, doi:10.1007/s11069-012-0294-2, 2012.

Kianirad, E., O'Donnell, A., Yang, W., Lai, T., and Mahdyiar, M.: Understanding and quantifying the impact of earthquake-triggered landslides in the Wellington area, Proc. Pac. Conf. Earthq. Eng., Paper 332, 2019.

https://doi.org/10.5194/egusphere-2025-5884
Preprint. Discussion started: 19 January 2026

Komar, P. D.: Shoreline evolution and management of Hawke's Bay, New Zealand: tectonics, coastal processes and human impacts, J. Coast Res., 26, 143–156, 2010.

Leonard, M., Burbidge, D. R., Allen, T. I., Robinson, D. J., McPherson, A., Clark, D., and Collins, C. D. N.: The challenges of PSHA in stable continental interiors: an Australian perspective, Bull. Seismol. Soc. Am., 104, 3008–3028, doi:10.1785/0120130248, 2014.

Liu, W., et al.: Global drought and severe drought-affected populations in warmer worlds, Earth Syst. Dyn., 9, 267–283, doi:10.5194/esd-9-267-2018, 2018.

Marzocchi, W., et al.: Principles of multi-risk assessment, European Commission Report, 2009.

Massey, C. I., de Vilder, S. J., Lukovic, B., Townsend, D. B., and Rosser, B. J.: District-scale landslide risk analysis for Kaikōura District, GNS Sci. Consult. Rep., 2021/89, 117 pp., 2021a.

Massey, C. I., Lukovic, B., Huso, R., Buxton, R., and Potter, S. H.: Earthquake-induced landslide forecast tool v2.0, GNS Sci. Rep., 2018/08, doi:10.21420/G2TP-9V, 2021b.

Massey, C., Lukovic, B., and Dellow, S.: A prototype Earthquake-Induced Landslide Forecast Tool for New Zealand, in: Coseismic Landslides, Springer, Singapore, 617–631, doi:10.1007/978-981-19-6597-5_17, 2022.

Moratalla, J. M., and Uma, S. R.: Probabilistic assessment of road accessibility under cascading hazards, Int. J. Disaster Risk Reduct., 91, 103692, doi:10.1016/j.ijdrr.2023.103692, 2023.

Pescaroli, G., and Alexander, D.: A definition of cascading disasters and cascading effects, Planet@Risk, 3, 58–67, 2015.

Petroliagkis, T. I., Voukouvalas, E., Disperati, J., and Bidlot, J.: Joint probabilities of storm surge, wave height and discharge, Publications Office of the EU, doi:10.2788/677778, 2016.

Power, W. L., Kaneko, Y., Becker, J. S., Lin, S.-L., Holden, C., and Mueller, C.: Hikurangi response plan: developing a scenario for an Mw 8.9 earthquake, GNS Sci. Consult. Rep., 2018/168, 39 pp., 2018.

Robinson, T., and Rosser, N.: Rapid landslide risk assessment of transport infrastructure, EGU General Assembly, Vienna, 2017.

Rollins, C., Rhoades, D. A., Rastin, S. J., Gerstenberger, M. C., Christophersen, A., Thingbaijam, K. K. S., and Williams, C. A.: Magnitude–frequency distributions for NZ earthquakes, GNS Sci. Rep., 2022/48, doi:10.21420/SXPX-8C68, 2022.

Rosser, B. J., and Dellow, G. D.: Assessment of liquefaction risk in Hawke's Bay, GNS Sci. Consult. Rep., 2015/186, 64 pp., 2017.

Sadegh, M., Moftakhari, H., Gupta, H. V., Ragno, E., Mazdiyasni, O., Sanders, B., Matthew, R., and AghaKouchak, A.: Multihazard scenarios for compound extremes, Geophys. Res. Lett., 45, 5470–5480, doi:10.1029/2018GL077317, 2018.

Scheele, F. R., Syed, Y., Hayes, J. L., Paulik, R., and Inglis, S.: Building inventory and vulnerability functions for NZ, GNS Sci. Rep., 2023/08, doi:10.21420/G34N-V958, 2023.

Suppasri, A., Mas, E., Charvet, I., Gunasekera, R., Imai, K., Fukutani, Y., Abe, Y., and Imamura, F.: Building damage characteristics and fragility curves of the 2011 GEJ tsunami, Nat. Hazards, 66, 319–353, doi:10.1007/s11069-012-0487-8, 2012.

Tilloy, A., Malamud, B. D., Winter, H., and Joly-Laugel, A.: A review of quantification methodologies for multi-hazard interrelationships, Earth Sci. Rev., 196, 102881, doi:10.1016/j.earscirev.2019.102881, 2019.

https://doi.org/10.5194/egusphere-2025-5884
Preprint. Discussion started: 19 January 2026

Tocchi, G., Cremen, G., Galasso, C., and Polese, M.: Development of a multi-risk index for Italy, Proc. 14th Int. Conf. Appl. Stat. Probab. Civ. Eng., Trinity College Dublin, 2023.

Tonkin & Taylor: Liquefaction vulnerability study, Report for the Earthquake Commission, Wellington, 50 pp., 2013.

United Nations ISDR: Hyogo Framework for Action 2005–2015, United Nations, Geneva, Document ISDR/2007/4, 2007.

Williams, C. A., Eberhart-Phillips, D., Bannister, S., Barker, D. H. N., Henrys, S., Reyners, M., and Sutherland, R.: Revised interface geometry for the Hikurangi subduction zone, Seismol. Res. Lett., 84, 1066–1073, doi:10.1785/0220130035, 2013.

Xin, D., Daniell, J. E., and Wenzel, F.: Review of fragility analyses for major building types in China, Nat. Hazards Earth Syst. Sci., 20, 643–672, doi:10.5194/nhess-20-643-2020, 2020.

Zhang, G., Robertson, P. K., and Brachman, R. W. I.: Estimating liquefaction-induced lateral displacements, J. Geotech. Geoenviron. Eng., 130, 861–871, 2004.

Zharikova, M., Sherstjuk, V., Boskin, O. O., and Dorovska, I.: Event-based approach to multi-hazard risk assessment, Int. Workshop Comput. Inf. Technol. Risk-Informed Syst., 2020.

Zhang, L. M., Zhang, S., and Huang, R. Q.: Multi-hazard scenarios and consequences in Beichuan, Eng. Geol., 180, 4–20, doi:10.1016/j.enggeo.2014.03.02, 2014.

8.0 Code availability

The code used to perform the analyses and generate the figures in this study is available from the authors upon reasonable request, with access provided through a private GitHub repository.

9.0 Data availability

The data used and/or generated during the study are also available from the authors upon reasonable request.

10.0 Competing interests

The authors declare that they have no competing interests related to this study.